FORMATION AND COLLAPSE OF INTERNAL TRANSPORT BARRIER

A. Fukuyama
Department of Nuclear Engineering,
Kyoto University,
Kyoto

K. Itoh
National Institute for Fusion Science,
Toki, Gifu

S.-I. Itoh, M. Yagi
Research Institute for Applied Mechanics,
Kyushu University,
Kasuga, Fukuoka

Japan

Abstract

A theoretical model of internal transport barrier (ITB) is developed. The transport model based on the self-sustained turbulence theory of the current-diffusive ballooning mode is extended to include the effects of $E \times B$ rotation shear. Delayed formation of ITB is observed in transport simulations. The influence of finite gyroradius is also discussed. Simulation of the current ramp-up experiment successfully described the radial profile of density, temperature and safety factor. A model of ITB collapse due to magnetic braiding is proposed. Sudden enhancement of transport triggered by overlaping of magnetic islands termnates ITB. The possibility of destabilizing global low-n modes is also discussed.

1. INTRODUCTION

The formation of internal transport barrier (ITB) has been observed in various operation conditions on large tokamaks. The significance on improved core plasma confinement is stimulating the effort to resolve the mechanism of formation and termination of ITB. The theory-based transport model [1] derived from the self-sustained turbulence of the current-diffusive ballooning mode (CDBM) successfully describes the formation of ITB in high $\beta_{\rm p}$ plasmas, in negative magnetic shear configurations as well as with off-axis current drive [2]. This model predicts the reduction of thermal diffusivity $\chi_{\rm CDBM}$ when the magnetic shear s is weak or negative and when the normalized pressure gradient α becomes large. The short wavelength fluctuations with $k \sim \omega_{\rm pe}/c$, which are predicted by the CDBM model, were detected recently by microwave scattering in TFTR plasmas with reversed magnetic shear [3]. We study here the effects of $E \times B$ rotation shear and finite gyroradius on ITB formation and a model of ITB collapse.

2. EFFECT OF $E \times B$ ROTATION SHEAR

In the presence of large ion pressure gradient and/or large toroidal rotation of plasma, radial electric field E_r is enhanced owing to the radial force balance on ions. The radial shear of the $E \times B$ poloidal rotation suppresses the fluctuations and leads to additional reduction of transport. This effect on the CDBM transport model was included in the analysis of surface transport barrier in H-mode plasmas[4]. It becomes prominent also near ITB and introduces another time scale of the phenomena.

We have carried out tokamak transport simulation using the thermal diffusivity derived from the CDBM transport model[2]

$$\chi_{\rm CDBM} = C\,\frac{F(s,\alpha,\kappa)}{1+G(s,\alpha)\,\omega_{E1}^2}\,\alpha^{3/2}\frac{c^2}{\omega_{\rm pe}^2}\,\frac{v_{\rm A}}{qR} \tag{1}$$

where the normalized pressure gradient, $\alpha \equiv -q^2R\,({\rm d}\beta/{\rm d}r)$, magnetic shear, $s \equiv (r/q)\,({\rm d}q/{\rm d}r)$, magnetic curvature, $\kappa \equiv -(r/R)(1-1/q^2)$ and $E\times B$ rotation shear, $\omega_{E1} \equiv (\tau_{\rm Ap}r/s)\,({\rm d}/{\rm d}r)(E_r/rB)$, and $\tau_{\rm Ap} = qR/v_{\rm A}$. The factor $F(s,\alpha,\kappa)$ represents the reduction due to weak or negative magnetic shear and large Shafranov shift, while the factor $1/(1+G\omega_{E1}^2)$ comes from the effect of $E\times B$ rotation shear. Explicit expressions of F and G are given in [2] and [4].

We solve the one-dimensional transport equations for a tokamak with circular cross section

$$\frac{\partial}{\partial t}n_s = -\frac{1}{r}\frac{\partial}{\partial r}r\,,_s + S_s, \quad \frac{\partial}{\partial t}\frac{3}{2}n_sT_s = -\frac{1}{r}\frac{\partial}{\partial r}r\,q_s + P_s, \tag{2}$$

$$\frac{\partial}{\partial t}B_\theta = \frac{\partial}{\partial r}\eta_{\rm NC}\left[\frac{1}{\mu_0}\frac{1}{r}\frac{\partial}{\partial r}rB_\theta - J_{\rm BS}\right] \tag{3}$$

where the radial fluxes are given by

$$,_s = n_sV_s - D\frac{\partial}{\partial r}n_s, \quad q_s = \frac{5}{2}n_sT_sV_s - \frac{3}{2}n_s\chi_s\frac{\partial}{\partial r}T_s \tag{4}$$

and the subscript s denotes the particle species. The transport coefficients are expressed as a sum of neoclassical contribution and $\chi_{\rm CDBM}$;

$$V_s = n_s\left(v_{\rm Ware} - 0.05\,\chi_{\rm CDBM}\,r/a^2\right), \quad D = D_{\rm NC} + 0.1\,\chi_{\rm CDBM} \tag{5}$$

$$\chi_{\rm e} = \chi_{\rm NC,e} + \chi_{\rm CDBM}, \quad \chi_{\rm i} = \chi_{\rm NC,i} + \chi_{\rm CDBM} \tag{6}$$

and fitting parameter C in Eq.(1) was chosen to be 8.

Figure 1(a) indicates typical time evolution of $T_{\rm e}(0)$ for tokamak plasma with $R = 3\,{\rm m}$, $a = 1.2\,{\rm m}$, $B = 3\,{\rm T}$, $I_{\rm p} = 1\,{\rm MA}$ and $n_{\rm e}(0) = 0.5\times10^{20}\,{\rm m}^{-3}$. In the case of heating power 5.5 MW, $T_{\rm e}(0)$ starts to increase about 0.9 s after the onset of heating. Without the effect of the rotation shear, such a delay of the transition was not observed. The delay time becomes shorter with the increase of the heating power. The reduction factor $1/(1+G\omega_{E1}^2)$ rapidly decreases near $r = 0.4\,{\rm m}$ just before the transition as shown in Fig. 1(b). Figure 2 illustrates the modification of the pressure profile and the thermal diffusivity before and after the transition. The ion thermal diffusivity at ITB is reduced to the level of neoclassical transport (Fig. 2(d)). It should be noted that, though the transition is triggered by the enhancement of the rotation shear, the thermal diffusivity is already lowered before the transition due to the factor $F(s,\alpha,\kappa)$. Lower plasma current and intense central heating make the transition easier.

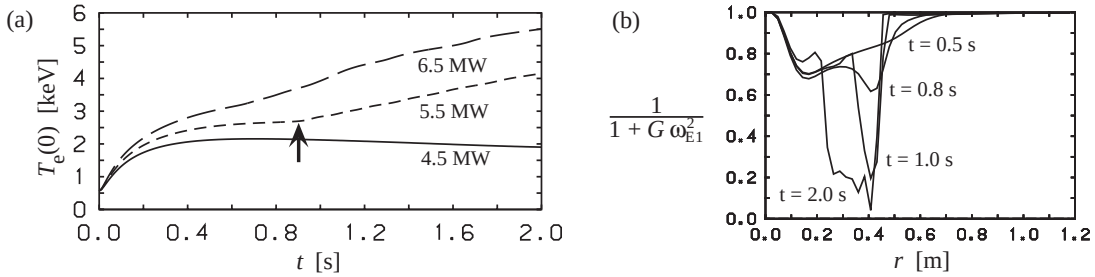

FIG. 1. Time evolution of the central temperature and the radial profile of the reduction factor due to the rotation shear.

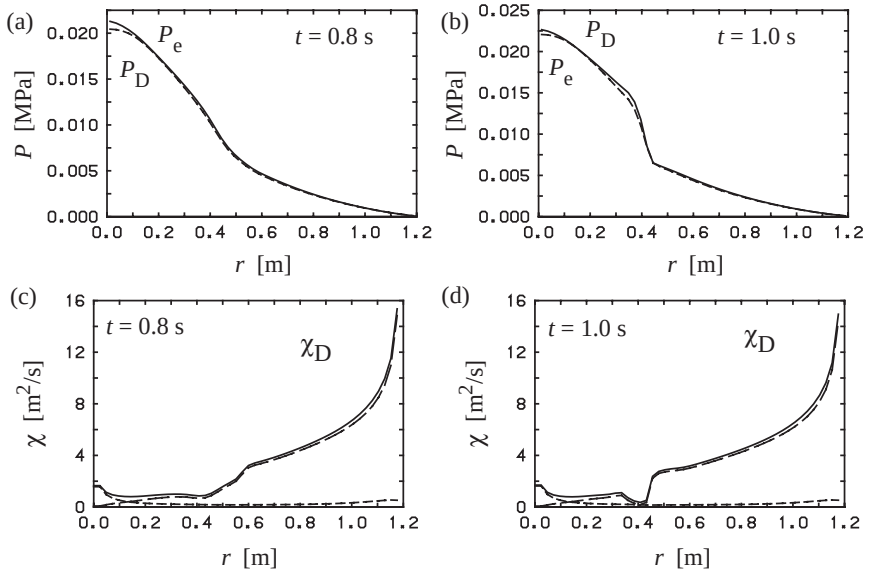

FIG. 2. Radial profile of the pressure and the ion thermal diffusivity before and after the transition

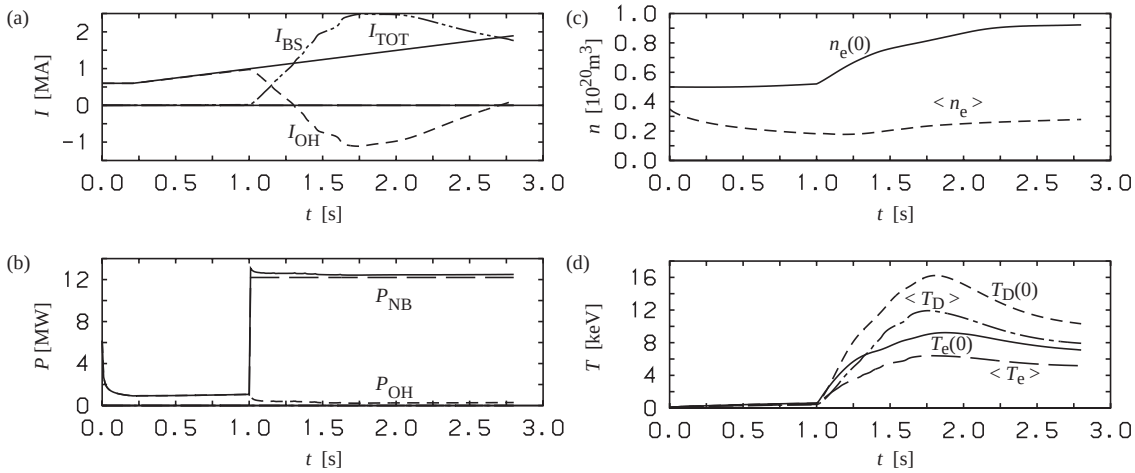

FIG. 3. Time evolution of plasma current (a), heating power (b), density (c) and temperature (d) in the negative shear configuration

We also simulated the confinement improvement in the negative magnetic shear configuration produced by current ramp-up. In order to simulate the evolution of the density profile, we have included the particle transport. Figure 3 shows time evolution of the plasma for $R = 3.15$ m, $a = 0.74$ m and $B = 4.28$ T. The plasma current was increased from 0.6 MA to 2 MA and NBI heating of 12 MW was switched on at $t = 1$ s. After the NBI heating started, the central and volume-averaged electron densities start to grow. The temperatures as well as the bootstrap current I_{BS} also start to increase but decline for $t > 1.8$ s. Radial profiles at $t = 1.8$ s are shown in Figure 4. The density, temperature and safety factor profiles are close to the experimental observation on JT-60U [5]. In order to reproduce long sustainment of ITB without current drive, however, further improvement of the transport model is required.

3. MODIFICATION DUE TO FINITE GYRORADIUS EFFECT

The present CDBM model does not distinguish the thermal diffusivities of electrons and ions. Since typical wave length of CDBM is comparable to or shorter than the ion gyroradius ρ_i, the finite gyroradius effect separates χ_e and χ_i. The finiteness of gyroradius also introduces the

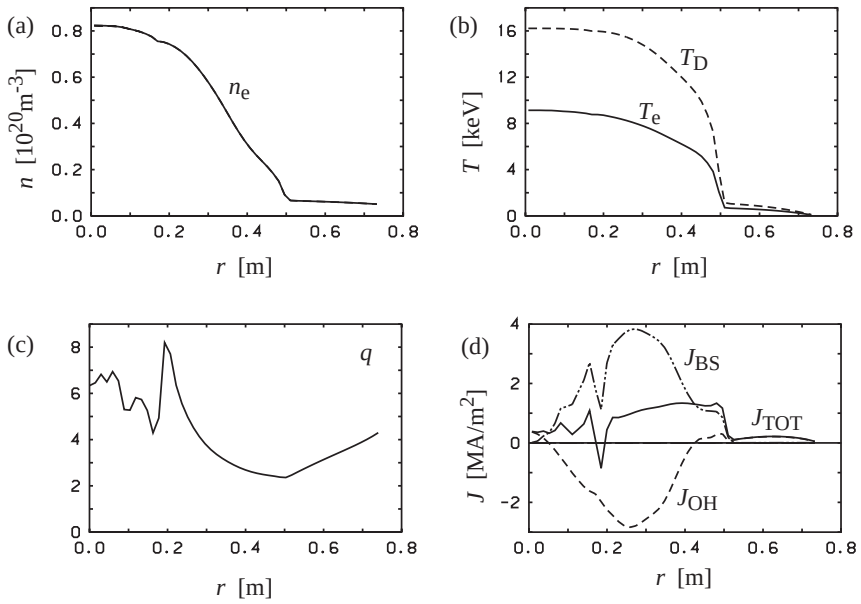

FIG. 4. Radial profile of density (a), temperature (b), safety factor (c) and current density (d) at $t = 1.8$ s in the negative shear configuration

coupling with diamagnetic drift of electrons and ions, which leads to real part of wave frequency and imaginary part of transfer rate $\chi k_\perp^2$.

The ballooning mode equation including the effect of ion gyroradius ρ_i and the ion drift frequency $\omega_{*\mathrm{i}}$ is written as

$$\frac{\mathrm{d}}{\mathrm{d}\eta}\frac{f}{-\mathrm{i}\omega+\lambda n^4q^4f^2}\frac{\mathrm{d}}{\mathrm{d}\eta}\tilde{\phi} + \left(\frac{\alpha_\mathrm{e}}{-\mathrm{i}\omega+\chi_\mathrm{e}n^2q^2f}+\frac{\alpha_\mathrm{i}\Lambda_0}{-\mathrm{i}\omega+\chi_\mathrm{i}n^2q^2f}\right)H(\eta)\tilde{\phi} + (\mathrm{i}\omega-\mathrm{i}\omega_{*\mathrm{i}}-\mu_\mathrm{i}n^2q^2f)f\Lambda_0\tilde{\phi} = 0 \quad (7)$$

where λ, χ_e, χ_i and μ_i are the current diffusivity, electron thermal diffusivity, ion thermal diffusivity and ion viscosity induced by the turbulence, respectively. n is the toroidal mode number, $\Lambda_0(b) = I_0(b)\mathrm{e}^{-b}$ and $b = n^2q^2\rho_\mathrm{i}^2/r^2$. The functions of the ballooning coordinates η are given by $H(\eta) = \kappa + \cos\eta + (s\eta - \alpha\sin\eta)\sin\eta$ and $f = 1 + (s\eta - \alpha\sin\eta)^2$.

Preliminary analysis indicates the enhancement of χ_e over χ_i by a factor of $1/\Lambda_0$. The mode frequency is in the direction of ion drift motion and the absolute value is much smaller than $|\omega_{*\mathrm{i}}|$. Comprehensive analysis of CDBM including finite gyroradius effect and E_r' suppression will be reported soon.

4. MODEL OF COLLAPSE

With the increase of the pressure gradient at ITB, the amplitude of turbulent fluctuation grows. When the amplitude of perturbation magnetic field exceeds a threshold value, the structure of the field lines becomes stochastic owing to the overlap of magnetic islands. In this state (M-mode)[6], strong enhancement of the thermal diffusivity leads to the collapse of ITB.

4.1. Catastrophe of transport coefficients

The nonlinear turbulence, which provides the formula Eq.(1) in the electrostatic limit, is subject to the turbulence-turbulence transition at a certain critical pressure gradient [7]. At this

threshold pressure gradient,

$$\alpha = \alpha_{\rm c} \sim \frac{(1+G\,\omega_{E1}^2)^{5/4}}{2\,F^{1/2}}\,\left[1+s^2F(1+G\,\omega_{E1}^2)^{1/2}\right]^2 \tag{8}$$

the associated magnetic fluctuation exceeds the threshold level that allows the overlapping of the microscopic magnetic island. If this microscopic island overlap takes place, the electron viscosity is selectively enhanced, in comparison with the ion viscosity, and the self-sustained turbulence becomes much more violent. As is schematically shown in Fig. 5(a), the turbulent transport coefficients, i.e., the thermal conductivity, current diffusivity, and ion viscosity increase. This strongly turbulent state has been called as "M-mode" [6,7]. The critical pressure gradient for the M-mode transition is illustrated in Fig. 5(b). It is approximately given by

$$\alpha_{\rm c} \sim \frac{s}{2} \qquad \text{(high shear limit)} \tag{9}$$

The M-mode transition does not occur in the weak shear region

$$s < 0.8 \tag{10}$$

The thermal transport coefficient in the M-mode is expressed as

$$\chi_{\rm e,M} \sim \frac{1}{1+G\,\omega_{E1}^2}\sqrt{\frac{m_{\rm i}}{m_{\rm e}}\alpha\beta_{\rm i}}\,\alpha^2\,\frac{c^2}{\omega_{\rm p}^2}\,\frac{v_{\rm te}}{qR} \tag{11}$$

$$\chi_{\rm i,M} \sim \frac{1}{1+G\,\omega_{E1}^2}\,\alpha^2\,\frac{c^2}{\omega_{\rm p}^2}\,\frac{v_{\rm te}}{qR} \tag{12}$$

where $m_{\rm i}/m_{\rm e}$ is the ion-to-electron mass ratio, $\beta_{\rm i} = \mu_0 n_{\rm i} T_{\rm i}/B^2$, $v_{\rm te}$ is the electron thermal velocity, and the suffix M indicates the M-mode turbulence. Compared to Eq.(1), $\chi_{\rm e}$ in the M-mode is enhanced by a factor of $\alpha\beta_{\rm i}m_{\rm i}/m_{\rm e}$, which is a few tens or so for usual parameters [7]. If the M-mode transition takes place, the enhanced thermal conductivity causes the reduction of the pressure gradient. It should be noticed that the turbulent transport has the nature of a hysteresis with respect to the pressure gradient, which is shown in Fig. 5(a). Once the state jumps to the M-branch, the turbulence level stays at the strongly turbulent state even if the pressure gradient becomes lower than the critical pressure, $\alpha \le \alpha_{\rm c}$. The M-state continues until the pressure gradient reaches the lower critical value

$$\alpha = \alpha_{\rm l} \sim \frac{1}{sF^{1/2}}\,\frac{1}{(1+G\,\omega_{E1}^2)^{1/4}} \tag{13}$$

As a result of this hysteresis nature, the pressure gradient drops from the critical value $\alpha_{\rm c}$ to the lower value $\alpha_{\rm l}$.

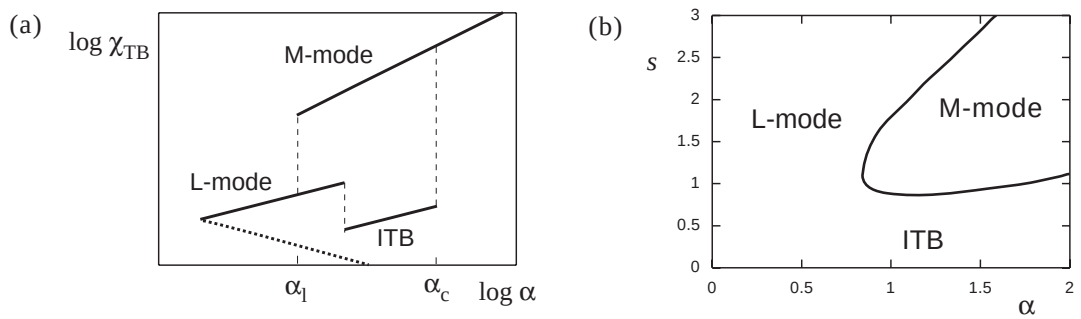

FIG. 5. Conceptual drawing of the thermal diffusivity as a function of the pressure gradient (a) and the critical gradient $\alpha_{\rm c}$ on the (α, s) plane (b).

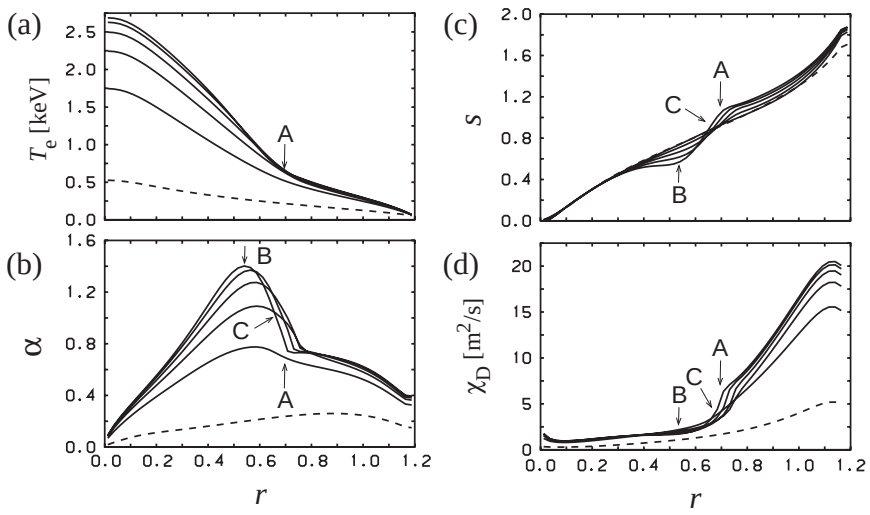

FIG. 6. Time evolution of the radial profile: (a) electron temperature T_e, (b) pressure gradient α, (c) magnetic shear s and (d) ion thermal diffusivity χ_D.

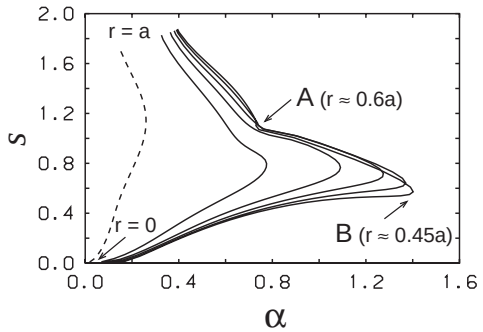

FIG. 7. Contour of the pressure gradient and the magnetic shear on the (α, s) plane.

The turbulence-turbulence transition, from the electrostatic one to the violent electromagnetic one, occurs within a very short time scale at $\alpha = \alpha_c$. The transition time from L-state/ITB to the M-state is given as

$$\tau_{\mathrm{transiton}} \sim \frac{\tau_{\mathrm{Ap}}}{\sqrt{\alpha}} \tag{14}$$

It should be noted that the time scale $\tau_{\mathrm{Ap}}/\sqrt{\alpha}$ is the typical time scale for the ideal MHD processes. The change of the state occurs within the so-called MHD time scale.

4.2. Comparison with simulation results

In order to illustrate the behavior of the pressure gradient, we present simulation results of ITB formation in the high β_p mode. Parameters are $R = 3\,\mathrm{m}$, $a = 1.2\,\mathrm{m}$, $I_p = 1\,\mathrm{MA}$, $n_e(0) = 5 \times 10^{19}\,\mathrm{m}^{-3}$ and the total heating power of $P_{\mathrm{heat}} = 10\,\mathrm{MW}$ for the deuterium plasma. About 100 ms after the start of the additional heating, the internal transport barrier starts to be formed. After 400 ms, the profile with internal transport barrier reaches the stationary state. Figure 6 shows the time evolution of the radial profiles. The temperature (a), pressure gradient profile (b), magnetic shear profile (c) and the turbulent transport coefficients (d) are shown for the Ohmic plasma (dotted line) and in the presence of the internal transport barrier. Arrow A indicates the ridge of the transport barrier (i.e., the interface between the regions of the improved confinement and the L-mode), arrow B for the peak of the pressure gradient. Within the surface $r \sim 0.6a$, the internal transport barrier is formed. The arrow C indicates the location where the crash starts to occur (as explained in Fig.8). In FIg. 7, radial profile of the pressure gradient

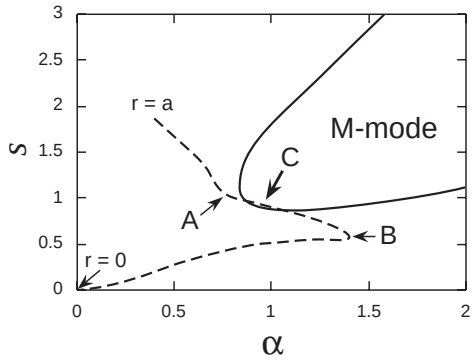

FIG. 8. Comparison of the simulation profile of $(\alpha(r), s(r))$ with the critical condition of the M-mode.

and magnetic shear, $(\alpha(r), s(r))$, are drawn on the (α, s) plane at the same time slices of Fig. 6. Arrows A and B indicate to the radial locations with arrows A and B in Fig. 6.

Figure 8 compares the critical condition with the typical profile in (α, s) plane obtained from transport simulation with ITB and threshold pressure $\alpha_{\rm c}(s)$. The locations indicated by A and B are the outer edge of ITB and the steepest gradient, respectively. When the profile $(\alpha(r), s(r))$ touches the critical line $\alpha_{\rm c}(s)$, transition to the M-mode occurs. The crash starts to occur at the location that is denoted by the thick arrow C. This radius is very close to the interface between the internal transport barrier and the L-mode region, denoted by arrow A. It is also shown that the contact with the critical curve takes place at the location of the large $\mathrm{d}\alpha/\mathrm{d}s$ value. The slope is negative, i.e.,

$$\frac{\mathrm{d}\alpha}{\mathrm{d}s} < 0 \tag{15}$$

This location is just inside the interface between the L-mode region and the transport barrier. The catastrophe of the internal transport barrier takes place at the outer region of the internal transport barrier.

4.3. Excitation of global mode

The enhanced electron viscosity in the M-mode is found to excite the global low-n mode, if the mode rational surface is close to ITB. Sudden jump of the growth rate in the time scale of $\tau_{\rm Ap}/\sqrt{\alpha}$ is predicted. If the M-mode transition takes place, the enhanced current diffusivity is given by

$$\lambda_{\rm M} \sim \frac{1}{1+G\,\omega_{E1}^2}\sqrt{\frac{m_{\rm i}}{m_{\rm e}}\alpha\beta_{\rm i}}\alpha^2\mu_0\,\frac{c^4}{\omega_{\rm p}^4}\,\frac{v_{\rm te}}{qR}. \tag{16}$$

This large current diffusivity may enhance the growth rate of various fluctuation modes. Consider the case that there exists a global mode, the mode rational surface of which is in the M-mode region. This global mode is selectively destabilized by this large current diffusivity. The current-diffusive mode has a growth rate, which is in proportion to $\gamma\tau_{\rm Ap}$ [8,9]. The formula of the growth rate has been given for the ballooning mode as [8]

$$\gamma\tau_{\rm Ap} = \left(\frac{\lambda}{\mu_0 r_{\rm s}^4}\right)^{1/5} m^{4/5}\alpha^{3/5}s^{-2/5} \tag{17}$$

where $r_{\rm s}$ is the mode rational surface and m is the poloidal mode number. The current diffusivity in the M-mode is given by Eq.(16), and gives the estimate

$$\left(\frac{\lambda}{\mu_0 r_{\rm s}^4}\right)^{1/5} \sim \alpha^{1/2}\left(\frac{c}{\omega_{\rm p} r_{\rm s}}\right)^{4/5} \tag{18}$$

Substituting this relation and $m = nq(r_s)$ into Eq.(17), one has

$$\gamma\tau_{Ap} \sim \left(\frac{c}{\omega_p r_s}\right)^{4/5} m^{4/5}\alpha^{11/10}s^{-2/5} \tag{19}$$

For the parameters of the experimental interest, e.g., $m = 3$, $\alpha \simeq 2$, $s \simeq 3$ and $c/\omega_p r_s \simeq 10^{-3}$, Eq.(19) provides the order of magnitude estimate as

$$\gamma\tau_{Ap} \sim 0.03 \tag{20}$$

This indicates that the growth rate of the order of $(3 \times 10^4 \sim 10^5)\,s^{-1}$ is expected, if the M-mode transition occurs, and the mode rational surface is located within the M-mode region. The change of the current diffusivity occurs within the time scale of (14). As a result, the change of the growth rate also takes place within the time scale of Eq.(14). In other words, the abrupt increase of the growth rate of the global mode onsets within the very short time, in the absence of the major variation of the global plasma parameters. The value of Eq.(20) is much larger than the linear resistive instability in the MHD-stable regions of parameters.

4.4. Irreversibility after the collapse

The M-mode is subject to a back-transition to the L-mode when the pressure gradient decreases below the lower critical pressure gradient. An avalanche of the back transitions in the radial direction is possible to occur [7,10]. After the end of avalanche in the plasma, the transport coefficient returns to the original one, Eq.(1), in the whole plasma column. In the lower branch of the transport coefficient, the thermal conductivity is low and the pressure gradient can start to grow again. The process can be repeated as a limit cycle, as is considered for the giant ELMs[7]. However, this is not always the case for the internal transport barrier. The density profile becomes much flatter, as a result of the collapse event. The flattened density profile usually leads to the broader heating profile. When the heating profile is broader, $r_{HW} \geq a/2$, the internal transport barrier is difficult to be formed[2]. This sensitivity to the heating profile is the key for the reversibility of the barrier formation after the crash. This explains the observations that the collapse is often a terminating event for the improved confinement.

This work is partly supported by the Grant-in-Aid for Scientific Research of the Ministry of Education, Science, Sports and Culture Japan, by the collaboration programme of the Advanced Fusion Research Centre of Kyushu University, and by the Collaboration programme of National Institute for Fusion Science.

REFERENCES

[1] ITOH, K., et al., Plasma Phys. Control. Fusion **35** (1993) 543.
[2] FUKUYAMA, A., et al., Plasma Phys. Control. Fusion **37**(1995) 611.
[3] WONG, K., et al., Phys. Lett. A **236** (1997) 339.
[4] ITOH, S.-I., et al., Plasma Phys. Control. Fusion **38** (1996) 1743.
[5] FUJITA T *et al.* 1996 *Proc. of 6th IAEA Conf. on Fusion Energy* IAEA-CN-64/A1-4
[6] ITOH, K., et al., Plasma Phys. Control. Fusion **37** (1995) 707.
[7] ITOH, S.-I., et al., Phys. Rev. Lett. **76** (1996) 920.
[8] YAGI M., et al., Phys. Fluids B **5** (1993) 3702.
[9] AYDEMIR, A. Y., Phys. Fluids B **2** (1990) 2135.
[10] KUBOTA, T., et al., Proc. of Int. Conf. on Plasma Physics (Nagoya, 1996) paper 9B19.